Available online at www.sciencedirect.com
SCIENCE DIRECT®
Solar Energy Materials & Solar Cells
ELSEVIER
Solar Energy Materials & Solar Cells 87 (2005) 311–316
www.elsevier.com/locate/solmat

Measurement of residual stress in EFG ribbons using a phase-shifting IR photoelastic method

M.C. Brito[a,*], J. Maia Alves[a], J.M. Serra[a], R.M. Gamboa[b], C. Pinto[a], A.M. Vallera[a]

[a]*Departamento de Fisica, Universidade de Lisboa, Departamento de Fisica/CFMC, Ed. C8 Campo Grande, 1749-016 Lisboa, Portugal*
[b]*ESTM—Instituto Politécnico de Leiria, Santuário Nossa Sra. dos Remédios, Apartado 126, 2524-909 Peniche, Portugal*

Received 15 May 2004; received in revised form 26 June 2004; accepted 2 July 2004
Available online 18 November 2004

Abstract

This paper reports on the measurement of residual stress in EFG silicon ribbons for solar cell applications using the phase-shifting infrared (IR) photoelastic method. The samples analysed were wafers cut from EFG octagons with 100 mm face width and from EFG 125 mm face-width octagon under development. Experimental results show that the distribution of residual stress in both types of samples is similar, within measurement uncertainties. The average residual stress in the samples is about 8 MPa. Maximum stresses of around 30 MPa are associated with twin and grain boundaries. Significant variations of stress along the growth direction, possibly related to buckling, were also measured.

Keywords: Silicon ribbons; EFG; Residual stress; Photoelasticity

1. Introduction

The growth of silicon ribbons for photovoltaic applications introduces stresses because of non-uniform temperature fields. Stress is critical in ribbon growth.

*Corresponding author. Tel.: +351 21 7500906; fax: +351 21 7500977.
E-mail address: mcbrito@fc.ul.pt (M.C. Brito).

0927-0248/$ - see front matter © 2004 Elsevier B.V. All rights reserved.
doi:10.1016/j.solmat.2004.07.028

It is associated with the generation of dislocations and permanent plastic deformations, which will limit the efficiency of solar cells made on these ribbons [1]. Furthermore, stress in silicon ribbons may lead to buckling, severely complicating the automation of solar cell processing. Finally, as residual stresses promote fracture by the propagation of microcracks occurring in the edges, large residual stresses can also lead to lower yield in solar cells processing [2]. The characterisation of residual stress in silicon ribbons is therefore of paramount importance.

In the past, the estimation of residual stress in EFG silicon ribbons has been deduced from the examination of deformation behaviour after scribing and fracturing [3] or directly measured using Shadow Moiré interferometry [2]. Other methods, such as linearly polarized cathodluminescence [4], polarized off-axis Raman spectroscopy [5] and nonlinear resonance ultrasonic vibrations [6] have also been used to determine residual stress in silicon wafers. The traditional infrared (IR) photoelastic method, an optical method based on the birefringence effect integrated over the sample thickness, has also been used to measure stress in thick (more than 1 mm) silicon wafers [7]. More recently, a variation of this method using a six-step phase-shifting technique for fractional fringe analysis, based on the method proposed by Patterson [8] for materials optically transparent to visible light, has been shown to be suitable for the determination of the residual stress in thin silicon wafers [9]. This method is particularly useful as an automatic characterisation tool that can be used for quality control and for diagnosing solar cell material growth.

2. Experimental method

In a series of experiments, we have measured the residual stress distribution in standard 100 mm EFG wafers (EFG100) as well as wafers from 125 mm octagons (EFG125), presently under development.

The residual stress was measured using the IR phase-shifting photoelastic method with constant photoelastic coefficient, which has been described in detail elsewhere [9]. The photoelastic coefficient depends on the direction of stress and on the direction of light propagation in the crystal. It has been shown that the relative error introduced by the variation of the photoelastic coefficient to the measured values is of the order of 30% [10].

The method assumes that the principal components of the refraction index are related to the principal components of the stress by the stress-optic law

$$n_1 - n_2 = C(\sigma_1 - \sigma_2), \tag{1}$$

where n_1 and n_2 are the principal components of the refraction index, σ_1 and σ_2 the principal components of the stress tensor and C is the photoelastic coefficient. The stress can thus be estimated by measuring the birefringence of the sample, e.g. the phase difference (Δ) between the fast and the slow axis of the sample (also known as

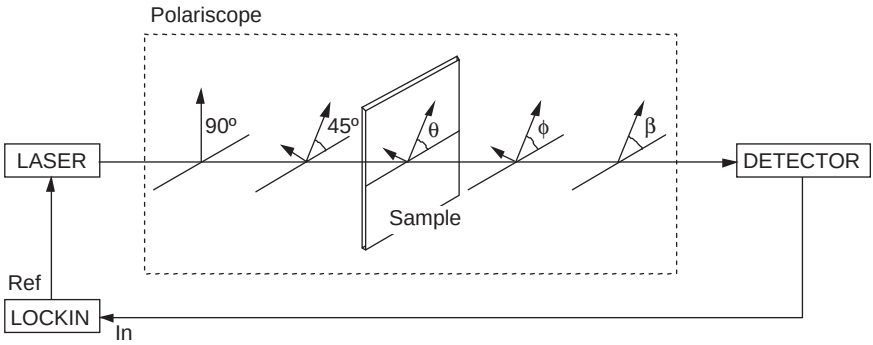

Fig. 1. Schematics of the experimental set-up for IR photoelastic stress measurement.

the isocromatic parameter):

$$\sigma_1 - \sigma_2 = \frac{\Delta\lambda}{Cd}, \tag{2}$$

where d is the sample thickness and λ the wavelength. The phase difference Δ is measured using a phase-shifting method, with six different polariscope configurations [9].

Fig. 1 shows the schematics of the experimental set-up. It includes the modulated light source followed by the polariscope, consisting of a linear polarizer and a quarter wave plate, in order to produce circularly polarized light; the sample, where the polarization of the light is shifted proportionally to the stress and its thickness; a second quarter wave plate and linear polarizer. Finally, the output signal is measured in a detector that is read by the lock-in amplifier.

The light source used is a 10 mW, 1310 nm IR laser diode Mitsubishi ML725B8F, electronically modulated at a frequency of 20 kHz. A HeNe laser was also installed for alignment purposes. The light detector is a high-speed InGaAs detector, DET410, from Thorlabs with an 800–1800 nm range. A Stanford RF880 lock-in amplifier measures the detector output signal. The scan used has a 0.3 mm step, smaller than the laser spot diameter, which is of the order of 1 mm.

3. Results and discussion

The measured distribution of residual stress in EFG ribbons is strongly correlated to the twin and grain boundaries across the sample, where maximum stresses of about 30 MPa were observed. This result is clearly seen in Fig. 2, which shows a typical shear stress measurement along a line transversal to the growth direction superimposed on a photograph of the sample where the defects can be seen.

Fig. 2 also shows that the variation of the isoclinic angle (defined by the direction of one of the principal components of the refraction index tensor with respect to the laboratory) is strongly correlated to the twin and grain boundaries but varies, in

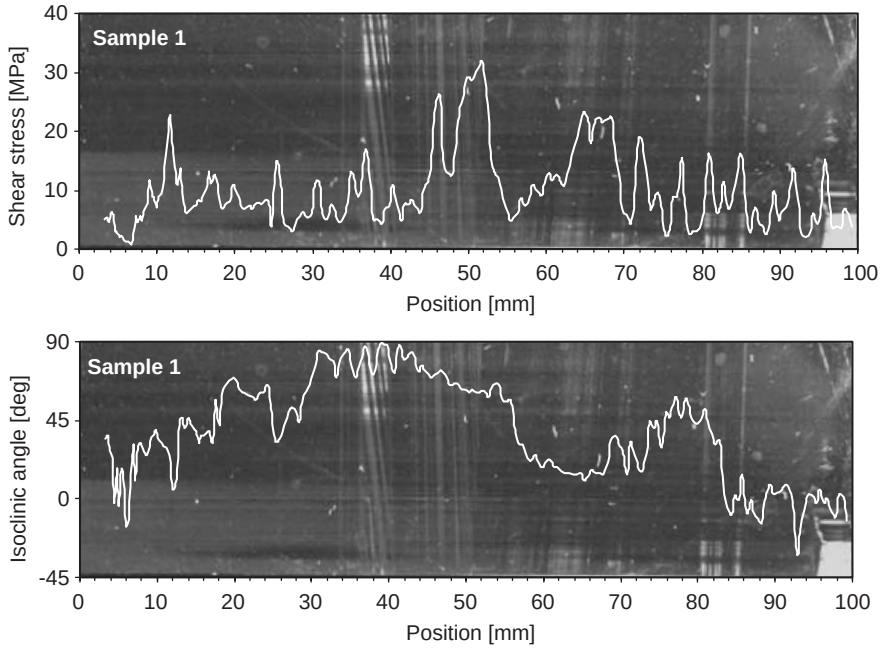

Fig. 2. Measured isoclinic angle and shear stress along line transversal to the growth direction on a 100 mm EFG wafer.

general, from around 0° near the edges of the ribbon to 90° in the central region, thus suggesting that there is tensile stress in the centre and compressive stress at the edges of the ribbons. This result is consistent with previous stress measurements on EFG ribbons using Shadow Moiré interferometry [2].

Fig. 3 shows the histograms of measured shear stress in the EFG100 and EFG125 samples along lines transversal to the direction of crystal growth. The stress distribution in both types of samples is similar, within statistical and measurement uncertainties. The average residual stress in all samples is around 8 MPa. As mentioned above, maximum stresses of about 30 MPa were measured around twin and grain boundaries, for both types of samples.

The distribution of stress in one single grain along the growth direction was also measured. We have concluded that the variation of stress can be quite significant (along a typical longitudinal line on a EFG125 mm the stress may vary from 5 to 25 MPa), although not necessarily in non-dislocated areas such as those where there are twins. This result can be related to buckling patterns which are periodic along the growth direction [11]. Buckles may not be visible on the wafer because stresses remain below the buckling threshold, in which case residual stress that are generated could still vary along the growth direction.

The measurements provide evidence that maximum residual stress is concentrated around twinned areas and grain boundaries. These structural defects are regions where there is a strong mismatch of the silicon lattice. However, the estimation of the

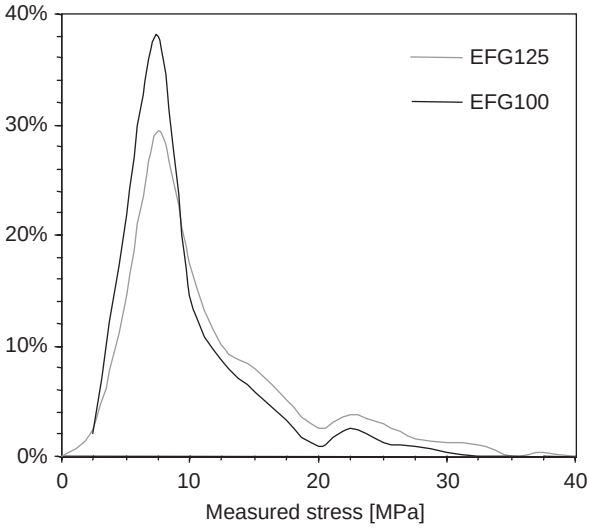

Fig. 3. Histograms of measured stress along lines transversal to the direction of growth on 100 mm EFG and 125 mm EFG wafer.

stress using the photoelastic method at, or close to, grain boundaries has to be taken with some caution since the stress-optic law may not hold due to the strong lattice mismatch. The stress distribution in silicon ribbons could be attributed to the distortions of the local lattice due to the elastic strain field of dislocations and lattice mismatch (volume expansion) of impuritiy atoms or precipitates [12].

Recent results on the distribution of impurities in EFG ribbons have suggested that, due to the relatively low generation of interstitial silicon from a reduced level of oxygen precipitation [13] and the high trapping efficiency by extended lattice defects [14] and substitutional carbon [15], there is a lack of interstitial silicon available for the formation of SiC. Instead, carbon forms perturbed C(3) configuration complexes with oxygen near structural defects such as grain boundaries and non-coherent twin boundaries [13,16]. On the other hand, oxygen also agglomerates at grain/twin boundaries and may form SiO_x clusters (with $x<2$) [17]. One overall effect of the accumulation of these impurities in the regions near structural defects is to extend the region of maximum stress from atomic distances (crystallographic origin) to a few microns (chemical origin).

4. Conclusions

The residual stress in EFG silicon wafers cut from EFG octagons with 100 mm face widths and from EFG 125 mm face-width octagons was measured using the IR phase-shifting photoelastic method. Experimental results show that the distribution of residual stress in both types of samples is similar, within statistical and measurement uncertainties.

There is evidence that there is tensile stress in the centre and compressive stress at the edges of the ribbons. The average residual stress along the samples is about 8 MPa and maximum stresses of around 30 MPa are concentrated around twin and grain boundaries. This experimental result could be explained by the accumulation of impurities, in particular carbon and oxygen, which is thought to occur in those regions.

Acknowledgements

The authors would like to thank Dr. W. Schmidt, from RWE Solar GmbH, for providing the samples and Dr. J.P. Kalejs for a very helpful discussion. This work was partly supported by SAPIENS and by a POCTI scholarship.

References

[1] J.C. Lambropoulos, J.W. Hutchinson, R.O. Bell, B. Chalmers, J.P. Kalejs, J. Cryst. Growth 65 (1983) 324–330.
[2] Y. Kwon, S. Danyluk, L. Bucciarelli, J.P. Kalejs, J. Cryst. Growth 82 (1987) 221–227.
[3] J.P. Kallej, A.A. Menna, R.W. Stormont, J.W. Hutchinson, J. Cryst. Growth 104 (1990) 14–19.
[4] Y. Tang, D.H. Rich, E.H. Lingunis, N.M. Haegel, J. Appl. Phys. 76 (1994) 3032–3040.
[5] G.H. Loechelt, N.G. Cave, J. Menendez, J. Appl. Phys. 86 (1999) 6164–6180.
[6] S. Ostapenko, I. Tarasov, Appl. Phys. Lett. 76 (2000) 2217–2219.
[7] S.R. Lederhandler, J. Appl. Phys. 30 (1959) 1631–1638.
[8] E.A. Patterson, Z.F. Wang, J. Strain Anal. 33 (1991) 1–15.
[9] M.C. Brito, J.C. Henriques, R.M. Gamboa, J.M. Serra, J. Maia Alves, A.M. Vallera, Proceedings of the 17th EPSEC, Munich, 2001, pp. 1862–1865.
[10] H.C. Liang, Y.X. Pan, S.N. Zhao, G.M. Qin, K.K. Chin, J. Appl. Phys. 71 (1992) 2863–2870.
[11] J.P. Kalejs, B.H. Mackintosh, T. Surek, J. Cryst. Growth 50 (1980) 175–192.
[12] H.J. Möller, C. Funke, A. Lawerenz, S. Riedel, M. Werner, Solar Energy Mater. Solar Cells 72 (2002) 403–416.
[13] J.P. Kalejs, J. Cryst. Growth 128 (1993) 298–303.
[14] B. Pivac, V. Borjanovic, I. Kovacevic, B.N. Evtody, E.A. Katz, Solar Energy Mater. Solar Cells 72 (2002) 165–171.
[15] R. Pinacho, P. Castrillo, M. Jaraiz, I. Martin-Bragado, J. Barbolla, H.J. Gossmann, G.H. Gilmer, J.L. Benton, J. Appl. Phys. 92 (2002) 1582–1587.
[16] F. Shimura, J. Appl. Phys. 59 (1986) 3251–3254.
[17] V. Borjanovic, I. Kovacevic, B. Santic, B. Pivac, Mater. Sci. Eng. B 71 (2000) 292–296.